Journal of Molecular Structure 1350 (2026) 144045

Contents lists available at ScienceDirect

Journal of Molecular Structure

journal homepage: www.elsevier.com/locate/molstr

Target-specific rhenium(I) tricarbonyl complexes as prospective pharmacological agents: Synthesis, X-ray crystallography, and *in vitro* anticancer evaluation

Lesetja V. Ramoba [a], Lucy W. Macharia [b], Suparna Chakraborty [b], Sharon Prince [b], Frederick P. Malan [c], Orbett T. Alexander [d], Amanda-Lee E. Manicum [a,*]

[a] Department of Chemistry, Tshwane University of Technology, P.O. Box X680, Pretoria 0001, South Africa
[b] Department of Human Biology, University of Cape Town, Anzio Road Observatory 7925, Cape Town, South Africa
[c] Department of Chemistry, University of Pretoria, 02 Lynnwood Road, Hatfield, Pretoria 0001, South Africa
[d] Department of Chemistry, University of the Western Cape, Bellville, Cape Town 7535, South Africa

ARTICLE INFO

Keywords:
Rhenium(I) tricarbonyl
Synthesis
X-ray crystallography
In vitro cytotoxicity

ABSTRACT

Rhenium tricarbonyl complexes have been investigated primarily due to their remarkable inhibitory effects against cancerous cells. This study presents the synthesis, solid-state crystallography, and *in vitro* biological evaluation of four rhenium(I) tricarbonyl complexes. The synthesized complexes: *fac*-[Re(Pico)$(CO)_3$(**L1**)] (**1**), *fac*-[Re(Pico)$(CO)_3$**L2**] (**2**), *fac*-[Re(5-Br-3-F-Pico)$(CO)_3$**L1**] (**3**) and *fac*-[Re(5-Br-3-F-Pico)$(CO)_3$**L3**] (**4**); where **L1** = 3,5-dimethyl-*1H*-pyrazole, **L2** = 3-(trifluoromethyl)-5-methyl-*1H*-pyrazole, and **L3** = 3,5-diphenyl-1H-pyrazole; were characterized with FT-IR, NMR (^{1}H and ^{13}C), UV-Vis spectroscopy, and single-crystal X-ray diffraction technique. Preliminary *in vitro* biological screening of these complexes at a concentration of 10 μM in DMSO (solvent) indicated that only complex **3** exhibited significant cell viability against HeLa (61.38 ± 9.55), CaSki (52.00 ± 2.78), and MDA-MB-231 (30.50 ± 4.72) cancer cell lines. Consequently, this complex was further evaluated for its half-maximal effective concentration (EC_{50}). The EC_{50} values for complex **3** were determined to be 45.6 ± 0.09 μM (selectivity index [SI] = 0.31), 19.87 ± 0.21 μM (SI = 0.71), and 6.0 ± 0.15 μM (SI = 2.36) against HeLa, CaSki, and MDA-MB-231 cells, respectively, with an EC_{50} value of 14.15 ± 0.23 μM against MRC-5 (normal human cells). Moreover, apoptosis and Western blot analyses reveal that complex **3** successfully induces apoptosis in cervical cancer cell lines (HeLa and CaSki) as well as in the triple-negative breast cancer cell line (MDA-MB-231).

1. Introduction

Cancer remains one of the leading health burdens globally, with statistics indicating that millions of new diagnoses along with deaths occur each year. For instance, in 2020, an estimated 19.3 million new cancer cases accompanied by 10.0 million cancer-related deaths were reported [1]. The most commonly diagnosed cancer types globally cover female breast cancer with 2.26 million cases, lung cancer (2.21 million), and prostate cancer (1.41 million). Furthermore, lung cancer led the way as the most common cause of cancer death, resulting in 1.79 million fatalities, followed by liver cancer (830 000) and stomach cancer (769 000) [1–6]. These high mortality rates have driven research into new and innovative treatments, including the development of metal-based drugs [7–12]. Rhenium(I) tricarbonyl complexes have gained interest in recent years as anticancer contenders due to the ideal nuclear properties such as half-lives of 90 h and 17 h, associated with ^{186}Re and ^{188}Re respectively, along with high energy emissions (E_{max} of 1.07 MeV for ^{186}Re and 2.12 MeV for ^{188}Re) [13]. Several rhenium(I) tricarbonyl complexes have also been evaluated as anticancer drug candidates in clinical trials [14,15]. Compared to traditional chemotherapeutics, these complexes offer distinctive properties that can be fine-tuned to improve efficacy and reduce toxicity towards normal cells [16]. Their ability to interact with biological targets at a molecular level introduces new approaches for targeted cancer therapy. Researchers are exploring various metal complexes, including those based on rhenium, due to their potential to disrupt cancer cell proliferation and induce apoptosis

* Corresponding author.
E-mail address: ManicumAE@tut.ac.za (A.-L.E. Manicum).

https://doi.org/10.1016/j.molstruc.2025.144045
Received 14 June 2025; Received in revised form 11 September 2025; Accepted 15 September 2025
Available online 16 September 2025

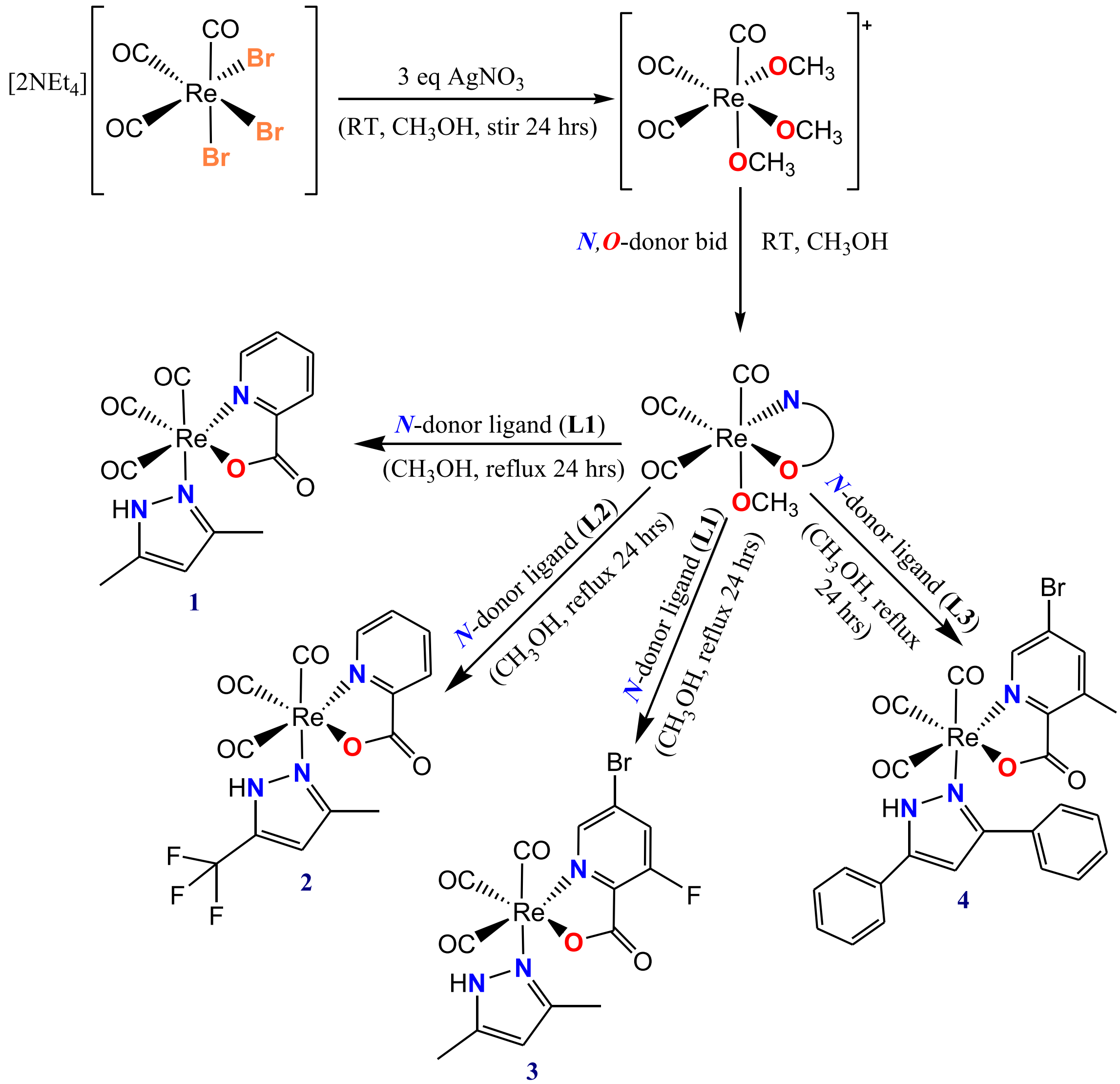

N,*O*-donor bid = 2-picolinic acid (Pico)
= 5-bromo-3-fluoropyridine-2-carboxylic acid (5-Br-3-F-Pico)

N-donor ligand = 3,5-dimethyl-*1H*-pyrazole (**L1**)
= 3-(trifluoromethyl)-5-methyl-*1H*-pyrazole (**L2**)
= 3,5-diphenyl-*1H*-pyrazole (**L3**)

Scheme 1. Synthetic route for the synthesized complexes (**1-4**).

[16–18]. Discoveries in this field could lead to groundbreaking advancements in cancer treatment, offering hope for more effective therapies. The ongoing exploration of these innovative metal drugs reflects the commitment of the medical community to combat cancer and improve patient outcomes.

The synthesis of rhenium(I) tricarbonyl complexes is accomplished using the *fac*-$[Re(CO)_3]^+$ synthon, which is notable for its capacity to generate a variety of coordination compounds. This metal core enables the coordination of various chelator ligands, ranging from monodentate to tridentate, thereby allowing for precise modulation of the resulting complexes' biological activity [19–22]. The carbonyl ligands within this metal framework contribute towards the stability of the complexes, which is significant for maintaining their integrity during biological interactions, an important feature in the mechanisms of action for anticancer therapies. This stability may lead to enhanced apoptosis or cell cycle disruption in cancer cells [23–25].

The coordination of picolinic acid analogs and the pyrazole ligands to the rhenium(I) tricarbonyl complexes enhances both the stability and reactivity of these compounds but also plays a critical role in defining their biological activity and therapeutic potential against cancer [26, 27]. In a noteworthy study, Matlou and co-workers (2023) explored the chemistry of rhenium(I) tricarbonyl complexes that comprise picolinic acid as the coordinating ligand. Their research revealed that these complexes demonstrated good and promising biological activity, exhibiting cytotoxic effects against HeLa cancer cells with a lethal concentration (LC_{50}) of 15.8 ± 4.9 μg/mL. Additionally, the complexes showed significant efficacy against the A549 cancer cell line, with an LC_{50} value of 20.9 ± 0.8 μg/mL [34]. This combination of chemical attributes positions them as promising candidates in the ongoing quest for effective metal-based anticancer therapies.

Rhenium(I) tricarbonyl complexes with pyrazole-based ligands have emerged as promising anticancer agents due to their favorable photophysical properties, structural flexibility, and tunable biological activity. Pyrazole ligands enable modulation of the electronic, steric, and lipophilic characteristics of rhenium complexes, allowing for fine-tuning of cellular uptake and cytotoxicity [49–51]. In a recent study, Łyczko *et al.* (2024) investigated pyrazole-containing rhenium(I) tricarbonyl complexes as potential anticancer agents. Their results indicated that several complexes displayed significant cytotoxic effects against specific cancer cell lines (IC_{50} < 20 μM against PC-3 and MCF-7), emphasizing the crucial role of ligand design, especially the inclusion of substituted pyrazoles, in influencing biological activity. This research underscores the increasing interest in rhenium-based complexes as viable candidates for metal-based chemotherapy [51].

Herein, four Re(I) tricarbonyl complexes are synthesized and characterized, in which the bidentate ligands are primarily *N,O′*-donor ligands, and selected pyrazole derivatives as the monodentate ligands. The *N,O′*-donor bidentate ligands employed in this study are 2-picolicolinic acid and its substituted counterpart 5-bromo-3-fluoropyridine-2-carboxylic acid. All the synthesized complexes were thoroughly characterized using various spectroscopic and analytical techniques for structural confirmation and subsequently evaluated for their biological activity.

2. Experimental

2.1. Materials and methods

Unless stated differently, all reagents used for the synthesis and analysis of products or compounds were obtained from Sigma Aldrich and Strem Chemicals (Newburyport, USA) and met analytical quality standards. The solvents and reagents used for synthetic purposes were applied as received, without further purification, except when the drying of compounds was necessary. All reactions that needed anaerobic or oxygen-free environments were conducted using argon or nitrogen gas under Schlenk line methods. Rhenium pentacarbonyl bromide, used in the first step for the synthesis of *fac*-$[NEt_4]_2[ReBr_3(CO)_3]$, was acquired from Strem Chemicals (USA). The compound *fac*-$[NEt_4]_2[ReBr_3(CO)_3]$ was synthesized according to the procedure described by Alberto *et al.* [28]. A PerkinElmer Lambda XLS + Ultraviolet/Visible (UV-Vis) spectrometer was used to collect the UV-Vis data using a 1.000 ± 0.001 cm quartz cuvette cell. For infrared (IR) characterization, a PerkinElmer FT-IR Spectrometer Spectrum, operating in the 4000–370 cm^{-1} region, was used to record the spectra. The IR is connected to a computer and has a built-in temperature cell regulator, accurate to 0.3°C. All the IR spectra of the synthesized complexes were recorded at room temperature. All Nuclear Magnetic Resonance (NMR) spectra were obtained with a Bruker 400 MHz NMR spectrometer at 400 MHz, using deuterated solvents ($CDCl_3$ and DMSO-d_6). Coupling constants, *J*, are reported in Hertz (Hz). For the *in vitro* biological study, the complexes showed solubility in DMSO, with no precipitates noted in the cell medium after being added to the cells. Furthermore, the UV-Vis solutions of the compounds were regularly recorded over several days to evaluate the stability of the complexes in DMSO.

2.2. Synthesis of fac-Re(I) tricarbonyl complexes

The rhenium(I) tricarbonyl complexes were synthesized following the established procedure described by Alberto *et al.* [28]. This synthesis utilized a "2 + 1" mixed ligand model, which begins with the coordination of bidentate ligands in the equatorial plane, followed by the attachment of a monodentate ligand in the sixth or axial position. The initial precursor, *fac*-$[NEt_4]_2[ReBr_3(CO)_3]$ (500 mg, 0.647 mmol) was dissolved in 10 mL of methanol. A solid addition of $AgNO_3$ (330 mg, 1.942 mmol) was made, and the mixture was stirred at room temperature for 24 h. The resulting greyish precipitate, AgBr, was filtered off, and an equivalent amount of picolinic acid or its substituted variant (80 mg, 0.647 mmol) was introduced to the filtrate, which was then stirred for another 24 h at room temperature. After that, *fac*-[Re(*N,O*-donor bid)$(CO)_3(HOCH_3)$] complexes (200 mg, 0.486 mmol) were dissolved by

Table 1
Crystal data and structure refinement for complex **1-4**.

Compound	1	2	3	4
Emp. formula	$C_{14}H_{12}N_3O_5Re$	$C_{14}H_9F_3N_3O_5Re$	$C_{14}H_{10}BrFN_3O_5Re$	$C_{24}H_{16}BrFN_3O_6Re$
CCDC Identifier	22358826	2293571	2431510	2431942
Form. weight (g.mol^{-1})	488.48	542.44	585.36	727.51
Crystal system	Monoclinic	Triclinic	Orthorhombic	Monoclinic
Space group	$P2_1/n$	$P\overline{1}$	$Pna2_1$	$P2_1/c$
Crystal color	yellow	yellow	yellow	yellow
Crystal morphology	blocks	blocks	blocks	blade
Crystal size (mm^3)	0.34 × 0.27 × 0.20	0.32 × 0.28 × 0.21	0.25 × 0.11 × 0.08	0.25 × 0.21 × 0.12
μ (mm^{-1})	7.825	7.375	17.154	12.522
a (Å)	6.5633(2)	8.9752(3)	16.3136(5)	13.33910(10)
b (Å)	14.8535(3)	9.1776(3)	16.0966(5)	16.9480(2)
c (Å)	16.1194(5)	10.4824(3)	6.4648(2)	10.89850(10)
α (°)	90	101.067(3)	90	90.0
β (°)	97.249(3)	100.738(3)	90	106.3000(2)
γ (°)	90	91.326(3)	90	90.0
Volume (Å^3)	1558.48(8)	830.99(5)	1697.61(9)	2364.06(4)
Z	4	2	4	4
ρ_{calc} (g cm^{-3})	2.078	2.168	2.290	2.044
F(000)	924	512	1096	1392
θ range (°)	2.737–31.160	2.717– 31.007	5.423–72.100	3.453–78.902
Index ranges	-8 ≤ h ≤ 7	-11 ≤ h ≤ 11	-20 ≤ h ≤ 20	- 16 ≤ h ≤ 16
	-18 ≤ k ≤ 17	- 11≤ k ≤ 11	- 19≤ k ≤ 19	- 16 ≤ k ≤ 21
	- 20 ≤ l ≤ 20	- 13 ≤ l ≤ 13	- 7 ≤ l ≤ 7	- 13 ≤ l ≤ 13
Radiation	MoK\a (λ =0.71073)	MoKα (λ = 0.71073)	CuKα (λ = 1.54184)	CuKα (λ = 1.54184)
Independent reflections	19918	18828	53853	27399
Unique reflections	3190	3397	3269	4990
R_{int}	0.0435	0.0983	0.0451	0.0647
Completeness to theta (%)	26.32, 99.91	52.6, 83	135.4, 99.8	71.98, 99.94
Data/Restraints/Parameters	3190/0/210	3397/0/ 236	3269/1/231	4990/0/ 332
Goodness of fit on F^2	1.080	1.042	1.033	1.109
Final R_1 indexes	0.0388	0.0316	0.0296	0.0308
wR_2 indices (all data)	0.0710	0.0751	0.0741	0.0854
Largest diffr. peak and hole (e.Å^{-3})	2.428 and -3.091	2.056 and -2.891	0.600 and -2.450	1.321 and -1.590

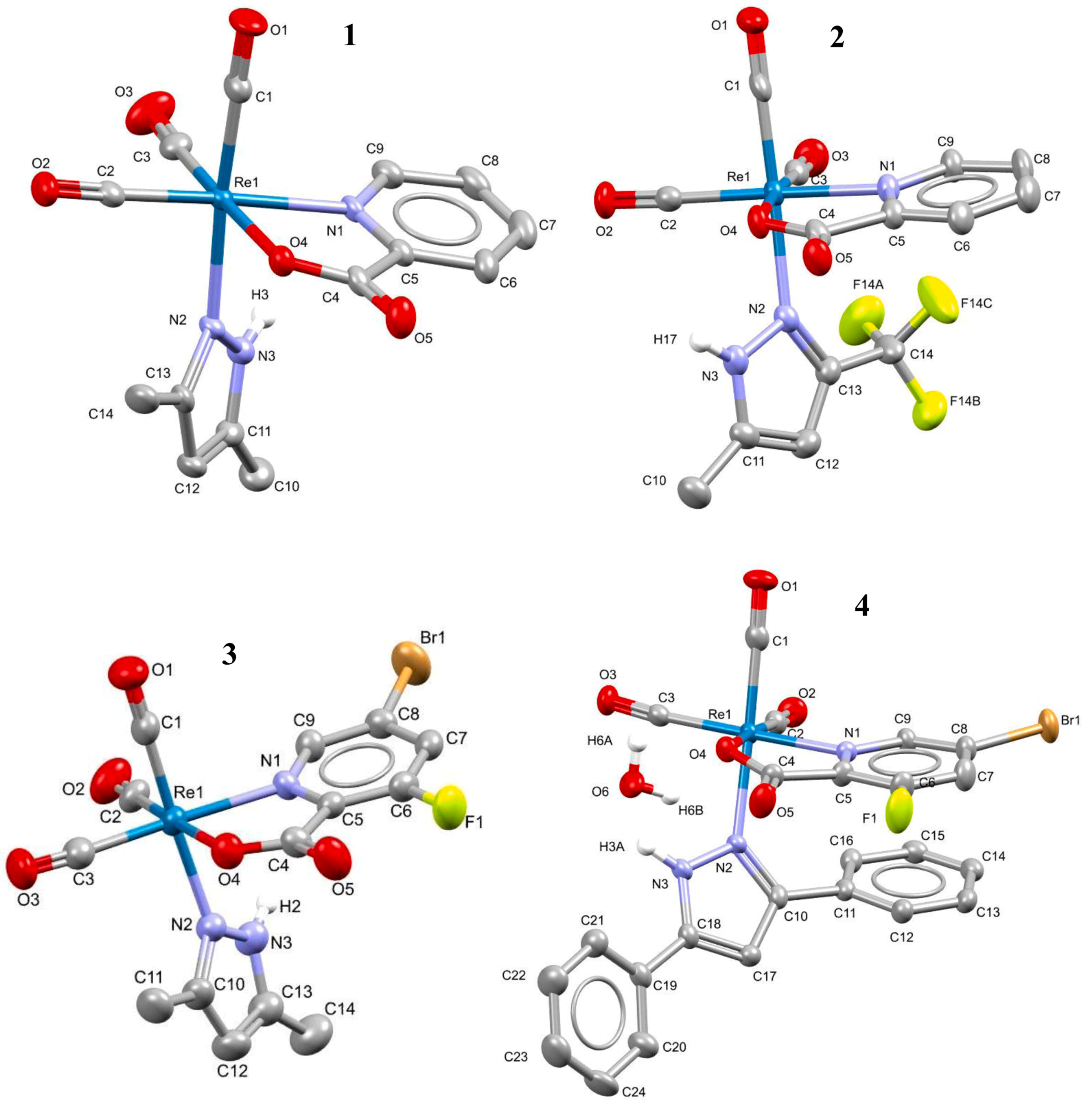

Fig. 1. Molecular representation of the crystal structures of complex **1, 2, 3,** and **4**. Thermal ellipsoids are plotted at 50 % probability. Hydrogen atoms of all complexes except for those on the imine nitrogen are omitted for clarity. Complex **4** is crystallized with a water guest molecule.

stirring in 6 mL of methanol. A solution containing 3,5-dimethyl-*1H*-pyrazole (**L1**), 3-(trifluoromethyl)-5-methyl-*1H*-pyrazole (**L2**), and 3,5-diphenyl-*1H*-pyrazole (**L3**) (73 mg, 0.486 mmol) in 2 mL of methanol was gradually added to the stirring solution. This mixture was allowed to stir at reflux temperature for 24 h. The resulting yellow solutions were then left to crystallize over several days. After five days, yellow crystals suitable for single-crystal X-ray diffraction were obtained. The final products were recovered in high yield, varying from 180 to 195 mg, corresponding to 68–79 %. An illustration of the synthetic route is given in Scheme 1.

2.2.1. Synthesis of fac-[Re(Pico)(CO)$_3$**L1**], **1**

^{1}H NMR (400.13 MHz, $CDCl_3$) δ_H (N-H) 11.30 (s, 1H), 8.91 (d, $J = 4$, 1H), 8.18 (m, 1H), 8.16 (d, $J = 4$, 1H) 7.59 (m, 1H), (-C=CH-) 5.78 (s, 1H), ($-CH_3$) 2.20 (s, 6H). ^{13}C NMR (101 MHz, $CDCl_3$) δ_C (-CO $_{(tricarbonyl)}$) 207.4, (CO$_{(ester)}$) 173.6, (-C=N-) 152.8, 152.2, (-C-N-) 150.9, 142.9, 140.14, 128.3, 128.0, (-C=C-$_{methine}$) 107.1, 104.1, (-C$_{(methyl)}$) 15.0, 11.4. FT-IR ν(CO, cm^{-1}): 2019, 1929, 1903, ν(-C=N-, cm^{-1}): 1550 . UV-Vis: $\lambda_{max} = 312$ nm, [0.0050] = 1995 M^{-1}.cm^{-1}. Yield: 190 mg, 79 %.

2.2.2. Synthesis of fac-[Re(Pico)(CO)$_3$**L2**], **2**

^{1}H NMR (400 MHz, DMSO-d$_6$) δ_H (N-H) 13.28 (s, 1H), 8.82 (d, $J = 4$, 1H), 8.31 (t, $J = 4$, 1H), 8.09 (d, $J = 8$, 1H), 7.83 (t, $J = 4$, 1H), (-C=CH-)

6.42 (s, 1H), (-CH_3) 2.28 (s, 3H). ^{13}C NMR (101 MHz, DMSO-d_6) δ_C (-CO $_{(tricarbonyl)}$) 198.1, 194.8, (CO$_{(ester)}$) 172.2, (-C=N-) 152.4, (-C-N-) 150.1, 141.7, 141.0, 129.3, 127.0, (-C=C-$_{methine}$) 102.6, (-C$_{(methyl)}$) 10.6. FT-IR ν(CO, cm^{-1}): 2025, 1933, 1891, ν(-C=N-, cm^{-1}): 1600. UV-Vis: λ_{max} = 292 nm, [0.0050] = 2150 M^{-1}.cm^{-1}. Yield: 180 mg, 68 %.

2.2.3. Synthesis of fac-[Re(5-Br-3-F-Pico)(CO)$_3$**L1**], **3**

^{1}H NMR (400 MHz, DMSO-d_6) δ_H (N-H) 12.79 (s, 1H), 9.05 (s, 1H), 8.61 (s, 1H), (-C=CH-) 6.31 (s, 1H), (-CH_3) 3.24 (s, 3H), 3.18 (s, 3H). ^{13}C NMR (101 MHz, DMSO-d_6) δ_C (-CO $_{(tricarbonyl)}$) 197.9, 197.8, 196.3, (CO$_{(ester)}$) 169.1, 168.4, (-C=N-) 158.7, (-C-N-) 152.5, 145.8, 143.7, 134.3, 134.1, 133.8, 124.8, 124.7, (-C=C-$_{methine}$) 107.1, 106.9, (-C$_{(methyl)}$) 14.4, 11.0. FT-IR ν(CO, cm^{-1}): 2022, 1907, ν(-C=N-, cm^{-1}): 1590. UV-Vis: λ_{max} = 332 nm, [0.0050] = 2147 M^{-1}.cm^{-1}, Yield: 180 mg, 68 %.

2.2.4. Synthesis of fac-[Re(5-Br-3-F-Pico)(CO)$_3$**L3**], **4**

^{1}H NMR (400 MHz, DMSO-d_6) δ_H 8.78 (s, 1H), 8.72 (s, 1H), 8.69, 7.86 (d, J = 8, 1H), 7.48 (t, J = 8, 1H), 7.36 (t, J = 8, 1H), (-C=CH-) 7.20 (s, 1H). ^{13}C NMR (101 MHz, DMSO-d_6) δ (-CO $_{(tricarbonyl)}$) 197.7, 194.4, (CO$_{(ester)}$) 168.9, 164.2, (-C=N-) 158.9, (-C-N-) 149.8, 147.0, 137.6, 137.5, 134.2, 134.0, 132.1, 129.3, 124.0, (-C=C-$_{methine}$) 100.3. FT-IR ν(CO, cm^{-1}): 2031, 1912, ν(-C=N-, cm^{-1}): 1600. UV-Vis: λ_{max} = 344 nm, [0.0025 M] = 1505 M^{-1}.cm^{-1}, Yield: 195 mg, 68 %.

2.3. Single-crystal X-ray crystallography

Single crystals of the complexes (**1-4**) were analyzed on a Rigaku XtaLAB Synergy R diffractometer, with a rotating-anode X-ray source and a HyPix CCD detector. Data reduction and absorption were carried out using the CrysAlisPro (version 1.171.40.23a) software package [29]. All X-ray diffraction measurements were performed at 150.0(2) K, using an Oxford Cryogenics Cryostat. All structures were solved by direct methods with SHELXT-2016 [30] and refined using the SHELXL-2016 [31] programs. All H atoms were placed in geometrically idealized positions and constrained to ride on their parent atoms. The X-ray crystallographic coordinates for all structures have been deposited at the Cambridge Crystallographic Data Centre (CCDC), with deposition numbers CSD 22358826, 2293571, 2431942, and 2431510. The data can be obtained free of charge from the Cambridge Crystallographic Data Centre via http://www.ccdc.cam.ac.uk/data_request/cif. The crystal data for **1-4** can be found in Table 1, while the molecular diagrams that illustrate the numbering scheme are presented in Fig. 1.

2.4. Biological studies

2.4.1. Cell culture

The MDA-MB-231 (triple-negative breast cancer), HeLa (HPV-18 cervical cancer), and MRC-5 (non-tumorigenic human fetal lung fibroblast) cells were grown in Dulbecco's Modified Eagle Medium (DMEM) (Gibco®, Life Technologies, New York). The CaSki (HPV-16 cervical cancer) and MCF-7 (estrogen receptor-positive breast cancer) cells were grown in Roswell Park Memorial Institute medium (RPMI) (Gibco®, Life Technologies, New York). The culture media were supplemented with 10 % Fetal Bovine Serum (FBS), 100 U/ml penicillin, and 100 µg/ml streptomycin for all the cancer cell lines but the media for the MRC-5 cells was supplemented with 20 % FBS. All cells were cultured at 37°C in a 5 % CO_2-95 % air-humidified incubator. Media was replaced every 2-3 days, and cells were routinely subjected to mycoplasma tests. Only mycoplasma-free cells were used in experiments.

2.4.2. Cell treatments

The complexes were dissolved in dimethyl sulfoxide (DMSO) (Merck 48856212719) to achieve a final stock concentration of 5 mM, heated at 100°C for 2 min, and then stored at room temperature for a maximum of 5 days before use. The 5 mM stock solutions were further diluted using a cell culture medium to attain a final experimental concentration of 10 µM, and a vehicle control (DMSO) of the equivalent highest compound concentration was prepared simultaneously. This concentration was selected because it is used by the National Cancer Institute (NCI, USA) in their initial screening of potential anticancer drug candidates [32]. Cisplatin (Pfizer Ltd, New York, USA) was included and used as the positive control for MCF-7, MDA-MB-231, CaSki, and HeLa cells. To establish the half maximal effective concentration (EC_{50}), the 5 mM stock solutions were further diluted using cell culture medium to attain final experimental concentrations (2, 4, 6, 8, and 10 µM for breast cancers and MRC-5) and (10, 20, 30, 40 and 60 µM) for cervical cancers and control (DMSO) of the same concentration was prepared simultaneously.

2.4.3. Cytotoxicity assay

The effects of the experimental complexes (**1 - 4**) on the viability of MDA-MB-231 and MCF-7 breast cancer cells, as well as the CaSki, and HeLa cervical cancer cells, were assessed using the 3-(4,5-dimethylthiazol-2-yl)-2,5-diphenyltrazolium bromide (MTT) assay (M21281G, Sigma-Aldrich), following the manufacturer's guidelines. Briefly, cells were seeded in 96-well plates and treated with the compounds or vehicle (DMSO) for 48 h, followed by the addition of 10 µL of the 5 mg/mL MTT solution to each well and incubated for further 4 h at 37°C. The mean cell viability was calculated as a percentage of the mean of the vehicle control. The absorbance at 600 nm was measured using a GloMax Explorer Multimode Microplate Reader GM3500 (Promega). At least two biological repeats in quadruplicate were performed from which the half maximal effective concentration (EC_{50}) was determined using GraphPad Prism v8.0.2 (GraphPad Software, California, USA). The selectivity index (SI) was determined by dividing the EC_{50} of the non-tumorigenic cell line (MRC-5) by the EC_{50} of the cancer cell line.

2.4.4. Apoptosis assay

Cells were treated for 48 h with **3** or cisplatin and then harvested by trypsinization and analyzed using the FITC Annexin V/Dead Cell Apoptosis kit (V13242; Thermo Fisher Scientific, Massachusetts, USA) according to the manufacturer's instructions. Briefly, treated cells were collected, washed with 1x PBS, counted, diluted to 1 × 106 cells/mL in a binding buffer and then stained for 15 mins with Annexin-V and propidium iodide (PI). A minimum of 2 × 104 cells/sample was analysed using a Becton Dickinson FACS Calibur flow cytometer (Becton Dickinson, New Jersey, USA). Unstained cells were included as a negative control and cells treated with 3 % formaldehyde (F8775, Sigma Aldrich, Missouri, USA) for 30 mins on ice and stained with Annexin-V and PI as positive controls to gate the flow cytometer for viable, early apoptotic, late apoptotic, and necrotic cell populations. Data acquired were analyzed using the FlowJo v10 software (Becton Dickinson, New Jersey, USA).

2.4.5. Western blot assay

Total protein lysates were prepared as described previously [33] and equal amounts of protein from each sample was separated using 8-15 % sodium dodecyl sulfate polyacrylamide gel electrophoresis (SDS-PAGE). The separated proteins were then transferred from the SDS-PAGE gels to WesternBrightTM NC nitrocellulose membranes (#230109-93, Advansta, USA). Following the blocking of membranes with 5 % skim milk or BSA, the membranes were incubated overnight at 4 °C with either mouse anti-β-actin (1:3000, sc-47778, Santa Cruz Biotechnology Inc, Texas, USA), rabbit anti-cleaved caspase 7 (1:1000,#8438S), or rabbit anti-PARP (1:1000, #9542S) all from Cell Signalling Technology. Thereafter, the membranes were incubated for 2 h with 1:5000 of horseradish peroxidase HRP-conjugated goat anti-rabbit IgG (H+L, #1706515) or goat anti-mouse IgG (H+L, #1706516) both from Bio-Rad, California, USA. To visualize the protein bands, SuperSignalTM West Pico PLUS chemiluminescence substrate (#YD371123, Thermo Scientific) and WesternBright TM ECM (#230719-95, Advansta, USA)

Table 2
A summary of the spectroscopic data for complexes **1 - 4**.

Complex	FT-IR υ_{CO} and $\upsilon_{C=N}$ (cm^{-1})	λ_{max} (nm)	ε ($M^{-1}.cm^{-1}$)	^{1}H-NMR (δ_{N-H}; ppm)	^{13}C-NMR ($\delta_{-C=N-}$; ppm)
1	υ_{CO} = 2019, 1929, 1903 $\upsilon_{C=N}$ = 1550	312	1 995	11.30	152.8
2	υ_{CO} = 2025, 1933,1891 $\upsilon_{C=N}$ = 1600	292	2 150	13.28	152.4
3	υ_{CO} = 2022, 1907 $\upsilon_{C=N}$ = 1590	332	2 147	12.79	158.7
4	υ_{CO} = 2031, 1912 $\upsilon_{C=N}$ = 1600	344	1 505	Absent	158.9

reagents were used, and visualization was done using the dark room or the ChemiDoc TM MP Imaging system (Bio-Rad). β-actin was used as a loading control and the band intensities were measured using the ImageJ software. Densitometry was performed using the image analysis software Fiji (Version 2.0.0-rc-68/1.52e) and protein expression levels were represented as a ratio of protein of interest/ β-actin and where appropriate normalized to the control sample.

2.5. Results and discussion

2.5.1. Synthesis and characterization

This study presents the synthesis and spectroscopic characterization of Re(I) tricarbonyl complexes (**1-4**). To obtain the intermediate product *fac*-$[Re(CO)_3(HOCH_3)_3]^+$, the rhenium precursor *fac*-$[NEt_4]_2[Re(CO)_3(Br)_3]$ was dissolved in methanol, followed by the addition of three equivalents of $AgNO_3$ to completely de-brominate the synthon in exchange with methanols and the nitrate counter-ion to balance the precursor charge. The coordination of the 2-picolinic acid bidentate ligand and its counterpart, 5-bromo-3-fluoropyridine-2-carboxylic acid, possesses a notable electronic impact on the coordination sphere of the metal core due to their anionic nature. This characteristic can significantly affect the electronic and steric properties within the complexes. Additionally, the exchange processes involving methanol and the pyrazole monodentate ligand systems taking part in the sixth position (axial) of the metal complex result in interesting dynamics in coordination compounds, allowing for variations in stability and reactivity. These interactions are crucial for understanding how changes in the ligand environment can influence the overall behavior of the metal complexes. The synthesized complexes yielded yellow precipitates in fairly high yields, ranging from 68 % to 79 %. A summary of the spectroscopic data for these complexes is illustrated in Table 2.

2.5.2. FT-IR characterization

The carbonyl stretching frequencies of these Re(I) complexes demonstrate significant similarities and align closely with other analogous structures documented in the literature, with values ranging from 2031 to 1891 cm^{-1} [34–36]. A trend in the frequencies of carbonyl stretching is observed as follows: **4** (2031) > **2** (2025) > **3** (2022) > **1** (2019). This trend can be explained by the presence of electron-withdrawing groups on the ligand backbone. These groups decrease the electron density at the Re(I) center, which limits the back-donation to the π* orbitals of CO. As a result, the C≡O bonds become stronger and require more energy to stretch. Notably, complexes **1** and **2** display three distinct carbonyl stretching bands, including one that manifests as a shoulder peak, unlike complexes **3** and **4**, which reveal only two carbonyl stretching bands, which correspond to symmetric and asymmetric carbonyl stretching. In these complexes, the displayed three distinct peaks are a clear indication of the fact that the facial carbonyl ligands are arranged in different electronic environments around the metal center, leading to loss of symmetry and resulting in individual FT-IR active stretching modes. Additionally, all the complexes exhibit an FT-IR medium peak around 1600 cm^{-1}, which is typical for the imine functional group within the pyrazole moiety coordinated in the sixth (axial) position of the metal center. All the FT-IR stretchings are heavily influenced by the substituents in the ligand backbone of both the monodentates and bidentate ligand systems [36].

2.5.3. UV-Vis characterization

The synthesized Re(I) tricarbonyl complexes described in this work exhibit UV-Vis absorption characteristics consistent with a low-spin d^6 configuration. Their lowest excited states are typically characterized by metal-to-ligand charge transfer (MLCT), with maximum absorption wavelengths (λ_{max}) ranging from 292 to 344 nm. The calculated molar absorptivity (ε) indicates that complexes **2** and **3** display stronger absorptions compared to complexes **1** and **4**, with values of 2 150 and 2 147 $M^{-1}.cm^{-1}$ for complexes **2** and **3**, respectively, while complexes **1** and **4** show values of 1 995 and 1 505 $M^{-1}.cm^{-1}$ [35]. Furthermore, a bathochromic shift is observed when transitioning from the complexes of picolinic acid (**1** and **2**) to those of the substituted analog, 5-bromo-3--fluoropyridine-2-carboxylic acid (**3** and **4**). The resulting red-shifted absorption profiles are significantly impacted by the presence of the electron-withdrawing substituents (bromine and fluorine) on the ligand backbone [37].

2.5.4. NMR characterization

The ^{1}H and ^{13}C NMR analyses of the Re(I) tricarbonyl complexes synthesized in this study were performed in deuterated chloroform and dimethyl sulfoxide at 25°C, as outlined in the experimental procedure section. The obtained NMR data indicate that the synthesized complexes are consistent with the proposed structures. Notably, the NMR chemical shifts of the coordinated ligands differ significantly from those of the free ligands. In the ^{13}C NMR spectra of these complexes, the coordination of the carboxylate group of the picolinic acid ligand is evidenced by the downfield shifts of its carbonyl signal. Specifically, there is a shift from 167.5 ppm in its uncoordinated state to an average of 172.9 ppm for complexes **1** and **2**. An interesting anomaly is observed for complexes **3** and **4** with the ligand 5-bromo-3-fluoropyridine-2-carboxylic acid. Their ^{13}C spectra do not exhibit significant downfield shifts upon coordination. The carbonyl resonances for these complexes appear at 169.1 and 168.9 ppm, respectively, which is near the chemical shift of the ligand in its uncoordinated state at 167.5 ppm. Conversely, the carbonyl groups in the *fac*-$[Re(CO)_3]^+$ exhibit average chemical shifts of around 200 ppm, which is typical for Re(I) tricarbonyl complexes. The specific shifts are as follows: 207.4 ppm for complex **1**; 198.1 and 194.8 ppm for complex **2**; 197.9, 197.8, and 196.3 ppm for complex **3**; and 197.7 and 194.4 ppm for complex **4**. Focusing on the imine carbon derived from the pyrazole moiety, the complexes exhibited resonances at 152.8, 152.4, 158.7, and 158.9 ppm for complexes **1** through **4**, respectively. Notably, the N–H proton resonance of complex **4** was absent in the ^{1}H NMR spectrum, likely due to rapid proton exchange with the solvent (DMSO-d_6) [48]. In contrast, the N–H proton peaks for complexes **1, 2**, and **3** were reported at 11.30, 13.28, and 12.79 ppm, respectively.

2.5.5. X-ray crystallography

The crystals for the molecular structures discussed in this study, identified as **1, 2, 3**, and **4**, were obtained through the slow evaporation of the solvent, as outlined in the synthetic procedure.

The molecular structures of the metal complexes feature the *fac*-$[Re(I)(CO)_3]^+$ moiety, in conjunction with an anionic picolinic acid bidentate ligand and its substituted analog, both coordinated in the equatorial plane. Furthermore, neutral monodentate ligands such as 3,5-dimethyl-*1H*-pyrazole (**L1**), 3,5-diphenyl-*1H*-pyrazole (**L2**), and 3-(trifluoromethyl)-5-methyl-*1H*-pyrazole (**L3**) occupy the sixth coordination site in the axial position. The coordination geometry surrounding the rhenium(I) metal center displays distortion, as evidenced by the O4-Re1-

Table 3
Selected bond lengths and angles for complex **1-4**.

Bond distances (Å)				
Complex	1	2	3	4
Re1-C1	1.927(5)	1.903(6)	1.912(7)	1.913(4)
Re1-C2	1.929(5)	1.925(5)	1.910(7)	1.917(4)
Re1-C3	1.919(6)	1.899(5)	1.922(6)	1.938(4)
Re1-N1	2.192(4)	2.183(4)	2.214(5)	2.187(3)
Re1-N2	2.197(4)	2.221(5)	2.203(5)	2.214(2)
Re1-O4	2.138(4)	2.131(3)	2.125(5)	2.146(4)
Bond angles (°)				
N1-Re1-O4	75.40(14)	75.59(14)	75.14(19)	74.74(11)
C1-Re1-N2	175.15(18)	176.44(17)	176.10(3)	172.77(14)

Table 4
Summary of percentage viability 48 h post-treatment with 10 μM of complex **1, 2, 3,** and **4** in various cancer cell lines.

Cell lines	Cervical Cancer		Breast Cancer	
Compounds	HeLa	CaSki	MCF-7	MDA-MB-231
Vehicle	100.00±4.60	100.00±2.90	100.00±3.04	100.00±6.18
1	90.02±5.31	93.06±0.88	98.30±3,63	100.81±6.10
2	-	-	-	-
3	61.38±9.55	52.00±2.78	96.78±5.55	30.50±4.72
4	97.68±7.99	85.79±6.17	94.17±5.28	97.87±2.42
Cisplatin	91.28±6.86	30.07±2.11	33.35±5.06	27.70±2.71

NB: Dashes (-) indicate that the complex was not screened against the selected cancer cell lines.
*vehicle = dimethyl sulfoxide (DMSO).

N1 bite angles measuring 75.40(14)° for complex **1**, 75.59(14)° for complex **2**, 75.14(19)° for complex **3** and 74.74(11)° for complex **4**. The Re-CO bond distances, approximately 1.90 Å, are consistent across all complexes, indicating their facial coordination with the metal ion. Additionally, the Re1-N bond distances are around 2.19 Å, slightly longer than the Re1-O bond distances of approximately 2.13 Å. This variation can be attributed to the differing donating abilities of nitrogen and oxygen toward the rhenium metal ion. One would expect the Re1-N1 and Re1-O4 bond distances in complexes **3** (2.214(5)and 2.125(5)) and **4** (2.187(3) and 2.146(4)) to be slightly longer than those in complexes **1** (2.192(4) and 2.138(4)) and **2** (2.183(4) and 2.131(3)). This expectation arises from the presence of the electron-withdrawing bromide and fluoride groups on the ligand backbone of the former complexes, compared to the latter. However, we do not observe this trend, possibly because the withdrawing effect is not significant. The observed bond distances and bite angles are in good agreement with previously reported structures in the literature [38–44]. Complexes **1** and **4** crystallized in the monoclinic crystal system (*P2₁/n* and *P2₁/c* respectively), while complex **2** crystallized in the triclinic $P\overline{1}$ space group, and complex **3** crystallized in the orthorhombic space group $Pna2_1$. The molecular arrangements in the unit cells for complexes **1** and **2** exhibit tail-to-tail and head-to-tail configurations, respectively, whereas complexes **3** and **4** display a mixed packing of head-to-head and tail-to-tail arrangements. All complexes are linked by intermolecular hydrogen bonds to stabilize themselves (see Table SI 1-4 and Figure SI 1). The selected bond distances and angles are presented in Table 3.

2.5.6. *Biological evaluation*

Three of the four complexes underwent *in vitro* anticancer screening against CaSki, HeLa cervical, MDA-MB-231, and MCF-7 breast cancer cell lines. Complex **2** was excluded from screening due to solubility issues in various solvents. Despite the highly asymmetric (triclinic space group) nature of **2**, when compared to others, and the induced high polarity by fluorine atoms in the pyrazolyl moiety, **2** was found to precipitate in DMSO over time. The cells were treated for 48 h with either the vehicle (DMSO) or 10 μM of complexes **1, 3,** and **4**, followed by MTT assays. Cisplatin was used as a reference drug in these evaluations, as it is a well-known chemotherapeutic agent for the treatment of these cancer types. Table 4 and Fig. 2 present the percentage cell viability of the screened complexes alongside the reference standards. Notably, complex **3** exhibited promising activity against the MDA-MB-231, HeLa, and CaSki cancer cell lines, showing cell viability percentages of 30.5 ± 4.72 %, 61.3 ± 9.55 %, and 52.0 ± 2.78 %, respectively. In contrast, complexes **1** and **4** were deemed inactive, with cell viability percentages exceeding 80 %.

Understanding the relationship between molecular structure and biological activity is essential for the rational design of effective metal-based therapeutics. In this study, we investigated the cytotoxic properties of a series of rhenium(I) tricarbonyl complexes, each bearing structurally varied ligands, to identify preliminary structure–activity trends. Although the scope of this investigation is constrained, notable correlations between ligand structure and antiproliferative activity are observed, offering early insights into the design principles that may underpin the biological efficacy of this class of compounds. Based on the observed preliminary *in vitro* results, the potency of the synthesized complexes increases from 2-picolinic acid (complex **1** with % cell viability = 90.02, 93.06, 98.30, and 100.81 against HeLa, CaSki, MCF-7, and MDA-MB-231) to the 5-bromo-3-fluoropyridine-2-carboxylic acid bidentate ligand system (complex **3** with % cell viability = 61.38, 52.00, 96.78, and 30.50 against HeLa, CaSki, MCF-7, and MDA-MB-231) while keeping the monodentate ligand constant (3,5-dimethyl-*1H*-pyrazole). The observed preliminary results suggest that the inclusion of these

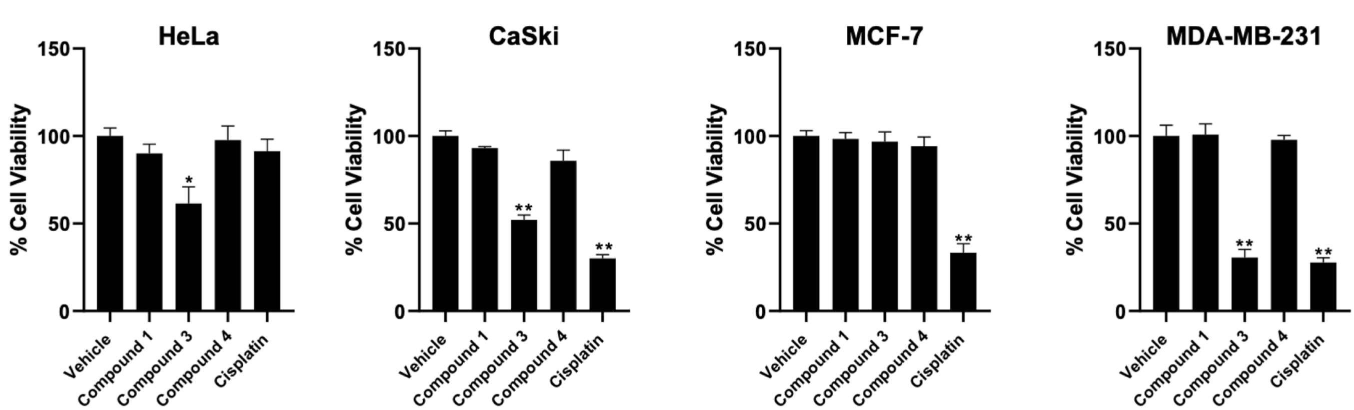

Fig. 2. Single-dose treatments of breast, and cervical cancer cell lines with **1, 3,** and **4** complexes. (A) HeLa, (B) CaSki cervical cancer, and (C) MCF-7, MDA-MB-231 breast cancer cell lines were treated with vehicle (DMSO) or 10 μM of **1, 3,** and **4** for 48 h followed by MTT cell viability assay. Graphs represent the mean cell viability ± SD of three independent experiments performed in quadruplicate. Data were analyzed using the parametric unpaired *t*-test by GraphPad Prism 8.0 software where *p < 0.05, **p < 0.01, ***0.001, and ****0.0001.

Table 5
EC_{50} values (μM) and selectivity indices (SI) of complex **3** in various cancer cell lines [45,46].

Compounds	Cell lines						
	HeLa		CaSki		MDA-MB-231		MRC-5
	EC_{50}	SI	EC_{50}	SI	EC_{50}	SI	
3	45.60 ± 0.09	0.31	19.87 ± 0.21	0.71	6.00 ± 0.15	2.36	14.15 ± 0.23
Cisplatin	66.03	0.11	17.46	0.45	13.98	0.61	15.0 ± 0.4

electron-withdrawing groups enhances the electrophilicity of the metal center or changes the overall electronic surroundings, possibly leading to stronger interactions with biological targets or affecting cellular uptake. This pattern indicates that adjusting the electronic properties of ligands can influence biological activity and serves as a valuable approach for optimizing compounds further.

However, the modification of the monodentate ligand from 3,5-dimethyl-*1H*-pyrazole (complex **3**) to 3,5-diphenyl-*1H*-pyrazole (complex **4** with % cell viability = 97.68, 85.79, 94.17, and 97.87 against HeLa, CaSki, MCF-7, and MDA-MB-231), while retaining the same bidentate ligand system (5-bromo-3-fluoropyridine-2-carboxylic acid), resulted in a significant decrease in cytotoxic activity. This decline could be attributed to the nucleophilic phenyl groups, which may impede cellular uptake or alter binding affinity to biological targets. These

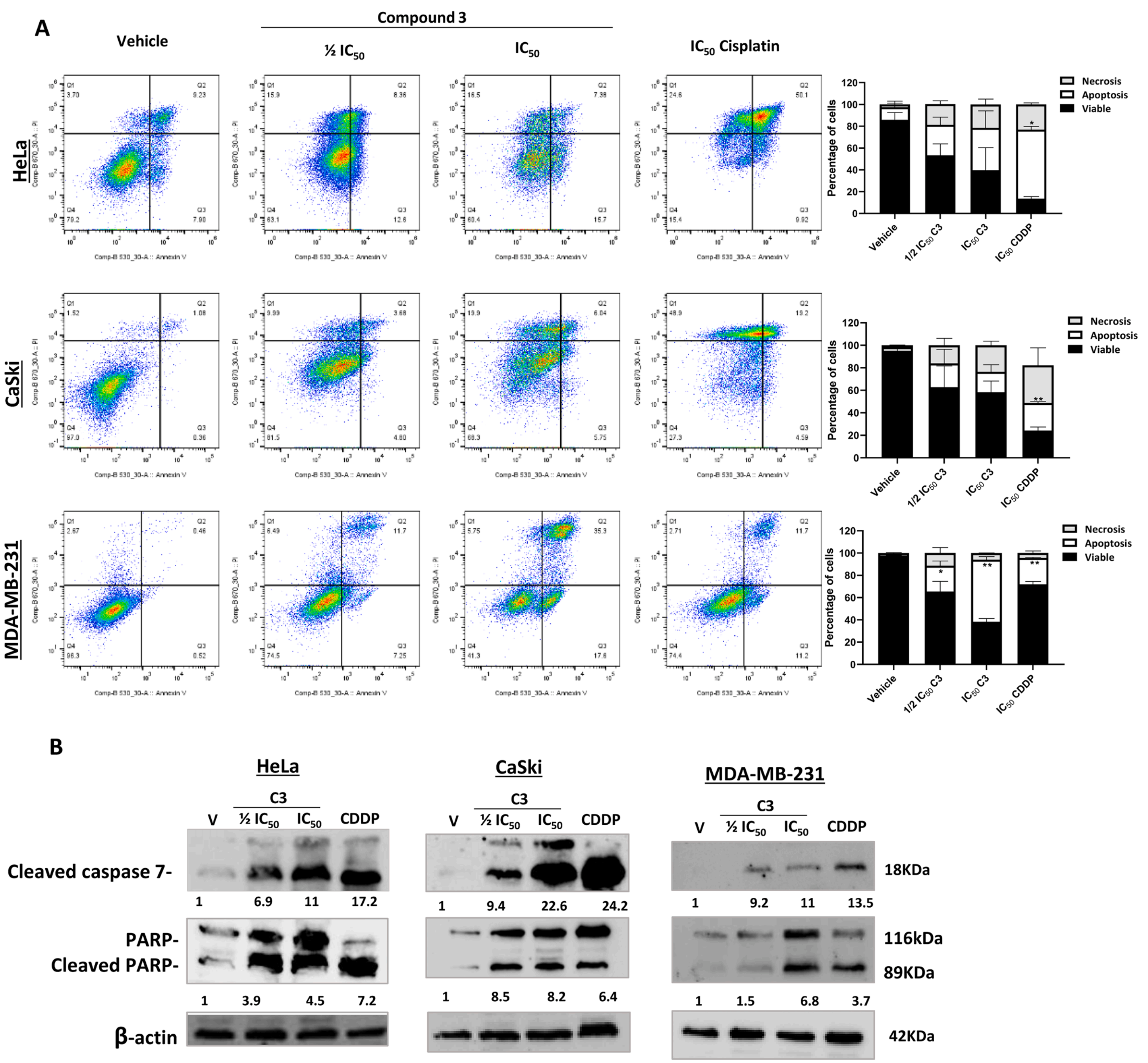

Fig. 3. (**A**) Annexin V-FITC/PI flow cytometry analysis of cells treated for 48 h with compound 3 or cisplatin (CDDP). Lower left-hand quadrant: viable cells; lower right-hand + upper right-hand quadrants: early and late apoptotic cells, respectively; upper left-hand quadrant: necrotic cells. (**B**) Western blot analysis of markers of apoptosis (cleaved caspase-7 and cleaved PARP) in cells treated as indicated. Graphs represent the mean cell viability ± SD of two independent experiments performed in quadruplicate. Data were analyzed using the parametric unpaired t-test by GraphPad Prism 8.0 software, where *p < 0.05, **p < 0.01, *** p < 0.001, and ****0.0001.

findings underscore the critical interplay between electronic and steric properties in modulating the biological efficacy of metal complexes. Furthermore, they provide a foundational framework for future design strategies aimed at optimizing anticancer potency.

Based on these results, only complex **3** was selected for further analysis to determine its half-maximal effective concentrations (EC_{50}) against the MDA-MB-231, HeLa, and CaSki cancer cell lines. See Table 5 for the percentage cell viability of these complexes.

To predict the selectivity potential of complex **3** the non-malignant MRC-5 cells were included in these experiments, and the selectivity indices (SI) for complex **3** in each cancer cell line were determined by dividing the EC_{50} for the MRC-5 cells by the EC_{50} values of the cancer cell line (see Table 5). The results showed that complex **3** exhibited an EC_{50} value of 14.15 ± 0.23 μM in MRC-5 cells and EC_{50} values of 45.60 ± 0.09 (SI = 0.31), 19.87 ± 0.21 (SI = 0.71), and 6.00 ± 0.15 (SI = 2.36) against HeLa, CaSki and MDA-MB-231 cells respectively. The observed EC_{50} values indicate that complex **3** is a promising therapeutic candidate when compared to the standard treatment, cisplatin. Moreover, the SI values obtained suggest that complex **3** is moderately selective ($2 < SI < 5$) towards MDA-MB-231 cancer cells while showing no selectivity ($SI < 2$) towards HeLa and CaSki cancer cells. The findings of this study further reinforce the conclusions of prior publications that emphasize the potential of rhenium complexes as promising anticancer agents. Notably, Moherane and co-workers (2022) reported a significant cytotoxic effect exhibited by certain rhenium-based complexes against MCF-7 cells (IC_{50} = 5.74 ± 2.5) and MDA-MB-231 cells (IC_{50} = 10.92 ± 2.3) [36,37,47]. A graphical representation of the EC_{50} of complex **3** can be found in Figure SI 5, while Table 5 shows the EC_{50} values (μM) and selectivity indices (SI).

2.5.7. Apoptosis and Western blot assays

To explore whether complex **3** induced apoptosis in the HeLa and CaSki cervical cancer cells and the MDA-MB-231 triple-negative breast cancer cells, annexin V-FITC/PI and flow cytometry analysis were performed. Fig. 3A shows that at both concentrations, complex **3** increased total apoptosis in all the cell lines tested. Furthermore, compared to the IC_{50} of the control drug cisplatin, the IC_{50} of **3** was more effective in inducing apoptosis in MDA-MB-231 cells, but less effective in inducing apoptosis in cervical cancer cell lines.

Western blotting with antibodies to key apoptotic markers confirmed that **3** induced apoptosis in the cervical cancer and breast cancer cell lines tested. Indeed, when the cells were treated with **3** there was an increase in the levels of cleaved caspase 7, the primary executioner caspase responsible for carrying out apoptosis, and cleaved PARP (see Fig. 3B).

2.6. Conclusion

Four pyrazole-based rhenium(I) tricarbonyl complexes were successfully synthesized with high yield and purity. These complexes underwent characterization using various spectroscopic techniques, including FT-IR, NMR (^{1}H and ^{13}C), and UV-Vis spectroscopy, and four molecular crystal structures were determined using single-crystal X-ray diffraction. The successful acquisition of these molecular crystal structures indicates that the “2+1” synthesis method employed in this study is reliable. A preliminary anticancer screening was conducted at a concentration of 10 μM for complexes **1, 3**, and **4** on several selected cancer cell lines, revealing that only complex **3** warranted further evaluation, specifically for determining the half-maximal effective concentration. The % cell viability of complexes **1** and **4** was found to be above 80 % against all the selected cancer cell lines, whereas complex **3** exhibited a % cell viability of 61.38±9.55 against HeLa, 52.00±2.78 against CaSki, 96.78±5.55 against MCF-7, and 30.50±4.72 against MDA-MB-231. The EC_{50} values obtained for complex **3** (EC_{50} = 45.60 ± 0.09, 19.87 ± 0.21, and 6.00 ± 0.15 against HeLa, CaSki, and MDA-MB-231 respectively) demonstrate its potential as a promising anticancer candidate when compared to the standard treatment, cisplatin. Furthermore, apoptosis and Western blot assays demonstrate that compound complex **3** effectively induces apoptosis in cervical cancer (HeLa and CaSki) and triple-negative breast cancer (MDA-MB-231) cell lines. This is evidenced by annexin V-FITC/PI staining and increased levels of cleaved caspase 7 and PARP. Although complex **3** was more potent than cisplatin in promoting apoptosis in MDA-MB-231 cells, it was less effective in the cervical cancer lines, suggesting cell-type-specific differences in sensitivity. Overall, complex **3** exhibits promising pro-apoptotic activity and potential as an anti-cancer agent, particularly in triple-negative breast cancer.

CRediT authorship contribution statement

Lesetja V. Ramoba: Writing – review & editing, Writing – original draft, Visualization, Methodology, Investigation, Formal analysis, Data curation, Conceptualization. **Lucy W. Macharia:** Methodology, Data curation. **Suparna Chakraborty:** Methodology, Data curation. **Sharon Prince:** Methodology, Data curation. **Frederick P. Malan:** Writing – review & editing, Supervision, Methodology, Data curation. **Orbett T. Alexander:** Writing – review & editing, Supervision, Methodology, Data curation. **Amanda-Lee E. Manicum:** Writing – review & editing, Supervision, Methodology, Data curation, Conceptualization.

Declaration of competing interest

The authors declare that they have no known competing financial interests or personal relationships that could have appeared to influence the work reported in this paper.

Acknowledgements

The authors would like to thank the National Research Foundation (Grant No: 129468), Tshwane University of Technology, University of the Western Cape, University of Pretoria, and South Africa, for institutional and financial support. Prof. Prince gratefully acknowledges and thank the University of Cape Town under the UCT Vision 2030 Grand Challenges Programme, the National Research Foundation of South Africa under a Competitive Programme for Rated Researchers, the International Centre for Genetic Engineering and Biotechnology (ICGEB) under a Collaborative Research Programme, the South African Medical Research Council (SAMRC) under a Self-Initiated Research Grant for financial support, as well as through the SAMRC Gynaecological Cancer Research Centre (GCRC). The views and opinions expressed are those of the author(s) and do not necessarily represent the official views of the SAMRC.

Supplementary materials

Supplementary material associated with this article can be found, in the online version, at doi:10.1016/j.molstruc.2025.144045.

Data availability

Data will be made available on request.

References

[1] L.I. Xiaoyu, H.U.A.N.G. Qing, W.U. Yumeng, H.U. Sheng, The Global cancer Statistics Report in 2022: a narrow spectrum summary and outlook, Cancer Res. Prev. Treat. 51 (5) (2024) 307–312.
[2] V. Kulothungan, K. Sathishkumar, S. Leburu, T. Ramamoorthy, S. Stephen, D. Basavarajappa, P. Mathur, Burden of cancers in India-estimates of cancer crude incidence, YLLs, YLDs and DALYs for 2021 and 2025 based on National Cancer Registry Program, BMC Cancer 22 (1) (2022) 527.
[3] R.L. Siegel, K.D. Miller, N.S. Wagle, A. Jemal, Cancer statistics, 2023, CA Cancer J. Clin. 73 (1) (2023) 17–48.

[4] J. Ferlay, M. Colombet, I. Soerjomataram, D.M. Parkin, M. Piñeros, A. Znaor, F. Bray, Cancer statistics for the year 2020: an overview, Int. J. Cancer 149 (4) (2021) 778–789.
[5] R.L. Siegel, K.D. Miller, H.E. Fuchs, A. Jemal, Cancer statistics, 2021, CA Cancer J. Clin. 71 (1) (2021) 7–33.
[6] Shimbre, M., Girum, T., & Mesfin, D. (2019). The burden of malignant neoplasms (cancer) in Ethiopia, 2000–16: analysis of evidences from Global Burden of Disease Study 2016 and global health estimates 2016.
[7] A.L. Lainé, C. Passirani, Novel metal-based anticancer drugs: a new challenge in drug delivery, Curr. Opin. Pharmacol. 12 (4) (2012) 420–426.
[8] N. Muhammad, Z. Guo, Metal-based anticancer chemotherapeutic agents, Curr. Opin. Chem. Biol. 19 (2014) 144–153.
[9] K.Benjamin Garbutcheon-Singh, M.P. Grant, B.W. Harper, A.M. Krause-Heuer, M. Manohar, N. Orkey, J.R. Aldrich-Wright, Transition metal based anticancer drugs, Curr. Top. Med. Chem. 11 (5) (2011) 521–542.
[10] M. Çeşme, A. Gölcü, I. Demirtaş, New metal based drugs: spectral, electrochemical, DNA-binding, surface morphology and anticancer activity properties, Spectrochim. Acta A: Mol. Biomol. Spectrosc. 135 (2015) 887–906.
[11] M.P.M. Marques, A.L. Batista de Carvalho, A.P. Mamede, A. Dopplapudi, S. Rudić, M. Tyagi, L.A. Batista de Carvalho, A new look into the mode of action of metal-based anticancer drugs, Molecules 25 (2) (2020) 246.
[12] H.Y. Khan, M.F. Ansari, S. Tabassum, F. Arjmand, A review on the recent advances of interaction studies of anticancer metal-based drugs with therapeutic targets, DNA and RNAs, Drug Discov. Today (2024) 104055.
[13] A.L. Manicum, O. Alexander, M. Schutte-Smith, H.G. Visser, Crystal structure of fac-(acetylacetonato-κ2 O, O′) tricarbonyl (tri-m-tolyl phosphane-κ P) rhenium (I), C29H28O5PRe, Z. Krist.-New Cryst. Struct. 233 (1) (2018) 23–25.
[14] Find trials. Available online: https://clinicaltrials.gov/(accessed on 20 April 2020).
[15] Maximum tolerated dose, safety, and efficacy of rhenium nanoliposomes in recurrent glioma—Full text view. Available online: https://clinicaltrials.gov/ (accessed on 21 April 2020).
[16] P. Collery, D. Desmaele, V. Vijaykumar, Design of rhenium compounds in targeted anticancer therapeutics, Curr. Pharm. Des 25 (31) (2019) 3306–3322.
[17] P.V. Simpson, M. Falasca, M. Massi, Properties and prospects for rhenium (i) tricarbonyl N-heterocyclic carbene complexes, Chem. Commun. 54 (88) (2018) 12429–12438.
[18] A. Harikrishnan, B.S. Supreetha, V. Veena, Mechanistic insight of rhenium-based compounds as anti-cancer agents. Topics in Anti-Cancer Research: Volume 10, Bentham Science Publishers, 2021, pp. 35–49.
[19] C. Olelewe, S.G. Awuah, Mitochondria as a target of third row transition metal-based anticancer complexes, Curr. Opin. Chem. Biol. 72 (2023) 102235.
[20] L.E. Enslin, K. Purkait, M.D. Pozza, B. Saubamea, P. Mesdom, H.G. Visser, M. Schutte-Smith, Rhenium (I) tricarbonyl complexes of 1, 10-phenanthroline derivatives with unexpectedly high cytotoxicity, Inorg. Chem. 62 (31) (2023) 12237–12251.
[21] E. Palma, J.F. Santos, C. Fernandes, A. Paulo, DNA-targeted complexes of Tc and re for biomedical applications, Chem.–Eur. J. 30 (13) (2024) e202303591.
[22] K. Ranasinghe, S. Handunnetti, I.C. Perera, T. Perera, Synthesis and characterization of novel rhenium (I) complexes towards potential biological imaging applications, Chem. Cent. J. 10 (2016) 1–10.
[23] Q. Qi, Q. Wang, Y. Li, D.Z. Silva, M.E.L. Ruiz, R. Ouyang, Y. Miao, Recent development of rhenium-based materials in the application of diagnosis and tumor therapy, Molecules 28 (6) (2023) 2733.
[24] L. Wallace, D.P. Rillema, Photophysical properties of rhenium (I) tricarbonyl complexes containing alkyl-and aryl-substituted phenanthrolines as ligands, Inorg. Chem. 32 (18) (1993) 3836–3843.
[25] S. Mundwiler, M. Kündig, K. Ortner, R. Alberto, A new [2+1] mixed ligand concept based on [99 (m) Tc (OH 2) 3 (CO) 3]+: a basic study, Dalton Trans. (9) (2004) 1320–1328.
[26] J. Karges, M.A. Giardini, O. Blacque, B. Woodworth, J.L. Siqueira-Neto, S. M. Cohen, Enantioselective inhibition of the SARS-CoV-2 main protease with rhenium (i) picolinic acid complexes, Chem. Sci. 14 (3) (2023) 711–720.
[27] D. Papagiannopoulou, Radiopharmaceutical applications of organometallic technetium and rhenium complexes, Curr. Inorg. Chem. (Discontin.) 2 (2) (2012) 228–247.
[28] R. Alberto, R. Schibli, R. Waibel, U. Abram, A.P. Schubiger, Basic aqueous chemistry of $[M(OH_2)_3(CO)_3]^+$(M= Re, Tc) directed towards radiopharmaceutical application, Coord. Chem. Rev. 190 (1999) 901–919.
[29] O. Rigaku, CrysAlis PRO Soft. Syst, Rigaku Corporation, Oxford, 2018.
[30] G.M. Sheldrick, SHELXT–Integrated space-group and crystal-structure determination, Acta Crystallogr. A: Found. Adv. 71 (1) (2015) 3–8.
[31] G.M. Sheldrick, Crystal structure refinement with SHELXL, Cryst. Struct. Commun. 71 (1) (2015) 3–8.
[32] A. Welsh, K. Serala, S. Prince, G.S. Smith, Selective targeting of regulated rhabdomyosarcoma cells by trinuclear ruthenium (II)–Arene complexes, J. Med. Chem. 67 (8) (2024) 6673–6686.
[33] S. Prince, T. Wiggins, P.A. Hulley, S.H. Kidson, Stimulation of melanogenesis by tetradecanoylphorbol 13-acetate (TPA) in mouse melanocytes and neural crest cells, Pigment Cell Res. 16 (1) (2003) 26–34.
[34] A.C. Wallace, R.A. Laskowski, J.M. Thornton, LIGPLOT: a program to generate schematic diagrams of protein-ligand interactions, Protein Eng. Des. Sel. 8 (2) (1995) 127–134.
[35] C. Triantis, T. Tsotakos, C. Tsoukalas, M. Sagnou, C. Raptopoulou, A. Terzis, M. Papadopoulos, Synthesis and characterization of *fac*-[M (CO) 3 (P)(OO)] and cis-trans-[M (CO) 2 (P) 2 (OO)] complexes (M= Re, 99mTc) with acetylacetone and curcumin as OO donor bidentate ligands, Inorg. Chem. 52 (22) (2013) 12995–13003.
[36] M.L. Matlou, F.P. Malan, S. Nkadimeng, L. McGaw, V.J. Tembu, A.L.E. Manicum, Exploring the in vitro anticancer activities of re (I) picolinic acid and its fluorinated complex derivatives on lung cancer cells: a structural study, JBIC J. Biol. Inorg. Chem. 28 (1) (2023) 29–41.
[37] K. Schindler, F. Zobi, Photochemistry of rhenium (i) diimine tricarbonyl complexes in biological applications, Chim. (Aarau) 75 (10) (2021), 837-837.
[38] V.L. Gantsho, M. Dotou, M. Jakubaszek, B. Goud, G. Gasser, H.G. Visser, M. Schutte-Smith, Synthesis, characterization, kinetic investigation and biological evaluation of re (I) di-and tricarbonyl complexes with tertiary phosphine ligands, Dalton Trans. 49 (1) (2020) 35–46.
[39] A. Brink, H.G. Visser, A. Roodt, Activation of rhenium (I) toward substitution in fac-[Re (N, O′-Bid)(CO)3(HOCH3)] by Schiff-base bidentate ligands (N, O′-Bid), Inorg. Chem. 52 (15) (2013) 8950–8961.
[40] R. Czerwieniec, A. Kapturkiewicz, R. Anulewicz-Ostrowska, J. Nowacki, fac-[Re(I)(CO)3]+ complexes with N∩ O− bidentate ligands, J. Chem. Soc. Dalton Trans. (18) (2002) 3434–3441.
[41] L.V. Ramoba, O.T. Alexander, H.G. Visser, A.L.E. Manicum, The crystal structure of fac-tricarbonyl (1, 10-phenanthroline-κ2 N, N′)-(pyrazole-κ N) rhenium (I) nitrate, C18H12O3N4Re, Z. Krist.-New Cryst. Struct. 235 (5) (2020) 1203–1205.
[42] L.V. Ramoba, O.T. Alexander, F.P. Malan, A.L.E. Manicum, The crystal structure of fac-tricarbonyl ((pyridin-2-yl) methanamino-κ2 N, N′)-((pyridin-2-yl) methanamino-κ N) rhenium (I) nitrate, C15H16O3N4Re, Z. Krist.-New Cryst. Struct. 238 (4) (2023) 709–711.
[43] L.V. Ramoba, O.T. Alexander, F.P. Malan, A.L.E. Manicum, The crystal structure of fa c-tricarbonyl (bis (3, 5-dimethyl-4 H-pyrazole)-κ1 N)-((nitrato)-κ1 O)-rhenium (I)—3, 5-dimethyl-4 H-pyrazole (1/1), C18H23N7O6Re, Z. Krist.-New Cryst. Struct. 239 (4) (2024) 735–737.
[44] W.K. Komane, P. Mokolokolo, B. Vatsha, A.L.E. Manicum, The crystal structure of fac-tricarbonyl (N′-benzoyl-N, N-diphenylcarbamimidothioato-κ2 S, O)-(pyrazole-κ N) rhenium (I)—Methanol (1/1) C26H23O4N4SRe, Z. Krist.-New Cryst. Struct. 236 (4) (2021) 767–769.
[45] A. Benamrane, B. Herry, V. Vieru, S. Chakraborty, S. Biswas, S. Prince, C. Marschner, B. Blom, Ionic ruthenium and iron based complexes bearing silver containing anions as a potent new class of anticancer agents, J. Organomet. Chem. 934 (2021) 121659.
[46] K. Serala, J. Bai, S. Prince, Pyrvinium pamoate alone and with gemcitabine exhibits anti-pancreatic cancer activity in 2D and 3D cell culture models, J. Cell. Mol. Med. 28 (23) (2024) e70222.
[47] L. Moherane, O.T. Alexander, M. Schutte-Smith, R.E. Kroon, P.P. Mokolokolo, S. Biswas, A.L.E. Manicum, Polypyridyl coordinated rhenium (I) tricarbonyl complexes as model devices for cancer diagnosis and treatment, Polyhedron 228 (2022) 116178.
[48] A. Majumdar, A. Kettani, E. Skripkin, D.J. Patel, Observation of internucleotide NH... N hydrogen bonds in the absence of directly detectable protons, J. Biomol. NMR 15 (1999) 207–211.
[49] D.I. Konovalov, A.A. Ivanov, Y.A. Vorotnikov, K.A. Brylev, I.V. Eltsov, N. V. Kuratieva, M.A. Shestopalov, Synthesis and luminescence properties of apically homoleptic octahedral rhenium clusters with pyrazole and 3, 5-dimethylpyrazole, Inorg. Chim. Acta 498 (2019) 119128.
[50] W.F. Mark-Lee, Y.Y. Chong, A.H. Lahuri, M.B. Kassim, Synthesis and solid-state structural elucidation of rhenium (i) complex with 1-cinnamoyl-3-(pyridin-2-yl) pyrazole, Malays. J. Anal. Sci. 24 (2020) 11–20.
[51] K. Łyczko, A. Pogorzelska, U. Częścik, M. Koronkiewicz, J.E. Rode, E. Bednarek, J. C. Dobrowolski, Tricarbonyl rhenium (i) complexes with 8-hydroxyquinolines: structural, chemical, antibacterial, and anticancer characteristics, RSC Adv. 14 (25) (2024) 18080–18092.